

# Origin of terminal voltage variations due to self-mixing in terahertz frequency quantum cascade lasers

ANDREW GRIER,<sup>1,5</sup> PAUL DEAN,<sup>1,6</sup> ALEXANDER VALAVANIS,<sup>1</sup>  
JAMES KEELEY,<sup>1</sup> IMAN KUNDU,<sup>1</sup> JONATHAN D. COOPER,<sup>1</sup>  
GARY AGNEW,<sup>2</sup> THOMAS TAIMRE,<sup>3</sup> YAH LENG LIM,<sup>2</sup>  
KARL BERTLING,<sup>2</sup> ALEKSANDAR D. RAKIĆ,<sup>2</sup> LIANHE H. LI,<sup>1</sup>  
PAUL HARRISON,<sup>4</sup> EDMUND H. LINFIELD,<sup>1</sup> ZORAN IKONIĆ,<sup>1</sup>  
A. GILES DAVIES,<sup>1</sup> AND DRAGAN INDJIN<sup>1,7</sup>

<sup>1</sup>*School of Electronic and Electrical Engineering, University of Leeds, Leeds LS2 9JT, UK*

<sup>2</sup>*School of Information Technology and Electrical Engineering, University of Queensland, Brisbane 4072, Australia*

<sup>3</sup>*School of Mathematics and Physics, The University of Queensland, Brisbane QLD 4072, Australia*

<sup>4</sup>*Materials and Engineering Research Institute, Sheffield Hallam University, Sheffield S1 1WB, UK*

<sup>5</sup>*atgrier4@gmail.com*

<sup>6</sup>*p.dean@leeds.ac.uk*

<sup>7</sup>*d.indjin@leeds.ac.uk*

**Abstract:** We explain the origin of voltage variations due to self-mixing in a terahertz (THz) frequency quantum cascade laser (QCL) using an extended density matrix (DM) approach. Our DM model allows calculation of both the current–voltage ( $I$ – $V$ ) and optical power characteristics of the QCL under optical feedback by changing the cavity loss, to which the gain of the active region is clamped. The variation of intra-cavity field strength necessary to achieve gain clamping, and the corresponding change in bias required to maintain a constant current density through the heterostructure is then calculated. Strong enhancement of the self-mixing voltage signal due to non-linearity of the ( $I$ – $V$ ) characteristics is predicted and confirmed experimentally in an exemplar 2.6 THz bound-to-continuum QCL.

Published by The Optical Society under the terms of the [Creative Commons Attribution 4.0 License](https://creativecommons.org/licenses/by/4.0/). Further distribution of this work must maintain attribution to the author(s) and the published article's title, journal citation, and DOI.

**OCIS codes:** (170.6795) Terahertz imaging; (120.3180) Interferometry; (140.5965) Semiconductor lasers, quantum cascade.

## References and Links

1. L. Li, L. Chen, J. Zhu, J. Freeman, P. Dean, A. Valavanis, A. G. Davies, and E. H. Linfield, "Terahertz quantum cascade lasers with >1 W output powers," *Electron. Lett.* **50**(2), 309–311 (2014).
2. S. Fatholouloumi, E. Dupont, C. Chan, Z. Wasilewski, S. Laframboise, D. Ban, A. Mátyás, C. Jirauschek, Q. Hu, and H. C. Liu, "Terahertz quantum cascade lasers operating up to ~ 200 K with optimized oscillator strength and improved injection tunneling," *Opt. Express* **20**(4), 3866–3876 (2012).
3. M. Tonouchi, "Cutting-edge terahertz technology," *Nat. photonics* **1**, 97–105 (2007).
4. Y. Lee, *Principles of terahertz science and technology* (Springer Science & Business Media, 2009).
5. P. Dean, A. Valavanis, J. Keeley, K. Bertling, Y. L. Lim, R. Alhathloul, A. D. Burnett, L. H. Li, S. P. Khanna, D. Indjin, T. Taimre, A. D. Rakić, E. H. Linfield, and A. G. Davies, "Terahertz imaging using quantum cascade lasers—a review of systems and applications," *J. Phys. D: Appl. Phys.* **47**(37), 374008 (2014).
6. D. Kane and K. A. Shore, *Unlocking Dynamical Diversity: Optical Feedback Effects on Semiconductor Lasers* (John Wiley & Sons, 2005).
7. E. Lacot, O. Jacquin, G. Roussely, O. Hugon, and H. G. De Chatellus, "Comparative study of autodyne and heterodyne laser interferometry for imaging," *J. Opt. Soc. Am. A* **27**(11), 2450–2458 (2010).
8. R. Lang and K. Kobayashi, "External optical feedback effects on semiconductor injection laser properties," *IEEE J. Quant. Electron.* **16**(3), 347–355 (1980).

9. J. A. Roumy, J. Perchoux, Y. L. Lim, T. Taimre, A. D. Rakić, and T. Bosch, "Effect of injection current and temperature on signal strength in a laser diode optical feedback interferometer," *Appl. Opt.* **54**(2), 312–318 (2015).
10. T. Taimre, M. Nikolić, K. Bertling, Y. L. Lim, T. Bosch, and A. D. Rakić, "Laser feedback interferometry: a tutorial on the self-mixing effect for coherent sensing," *Adv. Opt. Photon.* **7**(3), 570–631 (2015).
11. K. Bertling, Y. L. Lim, T. Taimre, D. Indjin, P. Dean, R. Weih, S. Hoffling, M. Kamp, M. von Edlinger, J. Koeth, and A. D. Rakić, "Demonstration of the self-mixing effect in interband cascade lasers," *Appl. Phys. Lett.* **103**, 231107 (2013).
12. R. Juškaitis, N. Rea, and T. Wilson, "Semiconductor laser confocal microscopy," *Appl. Opt.* **33**, 578–584 (1994).
13. A. Valavanis, P. Dean, Y. L. Lim, R. Alhathloul, M. Nikolic, R. Kliese, S. Khanna, D. Indjin, S. Wilson, A. Rakić, E. Linfield, and G. Davies, "Self-mixing interferometry with terahertz quantum cascade lasers," *IEEE Sensors J.* **13**(1), 37–43 (2013).
14. P. Dean, A. Valavanis, J. Keeley, K. Bertling, Y. Leng Lim, R. Alhathloul, S. Chowdhury, T. Taimre, L. H. Li, D. Indjin, S. J. Wilson, A. D. Rakić, E. H. Linfield, and A. Giles Davies, "Coherent three-dimensional terahertz imaging through self-mixing in a quantum cascade laser," *Appl. Phys. Lett.* **103**, 181112 (2013).
15. P. Dean, Y. L. Lim, A. Valavanis, R. Kliese, M. Nikolić, S. P. Khanna, M. Lachab, D. Indjin, Z. Ikonić, P. Harrison, A. D. Rakić, E. H. Linfield, and A. G. Davies, "Terahertz imaging through self-mixing in a quantum cascade laser," *Opt. Lett.* **36**(13), 2587–2589 (2011).
16. T. V. Dinh, A. Valavanis, L. J. M. Lever, Z. Ikonić, and R. W. Kelsall, "Extended density-matrix model applied to silicon-based terahertz quantum cascade lasers," *Phys. Rev. B* **85**(23), 235427 (2012).
17. H. Callebaut and Q. Hu, "Importance of coherence for electron transport in terahertz quantum cascade lasers," *J. Appl. Phys.* **98**, 104505 (2005).
18. M. Frančić, D. O. Winge, J. Wolf, V. Liverini, E. Dupont, V. Trinité, J. Faist, and A. Wacker, "Impact of interface roughness distributions on the operation of quantum cascade lasers," *Opt. Express* **23**(4), 5201–5212 (2015).
19. A. Grier, "Data associated with Origin of terminal voltage variations due to self-mixing in terahertz frequency quantum cascade lasers," University of Leeds data repository (2016) <http://doi.org/10.5518/77>.
20. A. D. Rakić, T. Taimre, K. Bertling, Y. L. Lim, P. Dean, D. Indjin, Z. Ikonić, P. Harrison, A. Valavanis, S. P. Khanna, M. Lachab, S. J. Wilson, E. H. Linfield, and A. G. Davies, "Swept-frequency feedback interferometry using terahertz frequency QCLs: a method for imaging and materials analysis," *Opt. Express* **21**(19), 22194–22205 (2013).

## 1. Introduction

Quantum cascade lasers (QCLs) are compact semiconductor sources of terahertz (THz) frequency radiation that are capable of emission powers of up to 1 W [1] and maximum operating temperatures of 200 K [2]. Owing to the transparency of many materials to THz radiation, coupled with its unique interaction with inter- and intra-molecular bonds in both organic and inorganic materials, a number of potential applications of these sources have been proposed including security screening, medical imaging, atmospheric science, and pharmaceutical monitoring [3,4]. In particular, the use of laser feedback interferometry (LFI) with QCL sources has received significant attention since it enables a wide range of coherent sensing applications without requiring a separate detector, and therefore simplifies experimental systems significantly [5].

LFI (based on the self-mixing (SM) effect) refers to the partial reinjection of the radiation emitted from a laser after reflection from a target; the injected radiation field interacts with the intra-cavity field causing a change in the operating parameters of the laser. These changes are required in order to maintain the field continuity across the laser facet-external cavity boundary, and in the case of semiconductor lasers, result in a measurable variation of the laser terminal voltage. This phenomenon has underpinned a wide range of sensing and imaging applications [6,7]. As such, an accurate physical understanding of the relationship between this SM voltage signal and the optical feedback from an external cavity is of great importance.

Typically the SM effect is described using the excess phase equation, obtained from the steady-state solution to the Lang–Kobayashi model [8–10]. This approach has been a mainstay of LFI for more than three decades, and even though the model was developed for a generic diode laser, the resulting variation of the self-mixing signal, with respect to external cavity length (or small frequency shifts) agrees remarkably well with experimental observations for all semiconductor lasers including QCLs and interband cascade lasers (ICLs) [11]. However, this model does not predict the magnitude of the SM voltage as a function of feedback level and the laser bias conditions. Experimental studies show that this signal is strongly dependent on the

laser structure, and can vary from the microvolt level for diode lasers to the millivolt level for THz QCLs.

To address this problem we have developed a comprehensive model that accounts for the laser structure in order to obtain quantitative information about the expected magnitude of the self-mixing voltage signal in THz QCLs. Whilst the Lang–Kobayashi model enables the dynamic state populations and light interaction to be modelled, a linear relationship between the change in intracavity light power,  $\Delta P$ , and terminal voltage variation  $V_{SM}$  is commonly assumed [12–14], i.e.

$$V_{SM} \propto \Delta P. \quad (1)$$

However, this assumption is not strictly applicable to QCL structures since carrier transport is dominated by the mechanisms of electron subband alignment, intersubband scattering, and photon driven transport between subbands with energy separations that change with applied bias (terminal voltage). Indeed, previous experimental observations based on a bound-to-continuum (BTC) QCL structure (see Fig. 2(b) in Ref. [15]) have shown SM voltage signal to be greatest near threshold and to decrease with greater driving currents, which suggests a non-linear relationship between  $V_{SM}$  and optical power,  $P$ . Further evidence of the limitation of this conventional approach is shown in the present work, in which we demonstrate a QCL device that departs significantly from the assumed linear behavior. We observe, both theoretically and experimentally, strong enhancement of the self-mixing signal in regions where the local gradient of the  $I$ – $V$  curve (differential resistance) increases.

Here we use an extended density matrix (DM) formalism to calculate the current–voltage characteristics of a BTC QCL emitting at 2.6 THz and predict the effect of feedback variation on the terminal voltage at a fixed drive current. The density matrix approach is capable of including coherent transport due to tunnelling as well as the effect of the cavity light field on current during lasing. This approach is shown to predict well the magnitude of the experimental self-mixing signal. The full details of the DM model are described in Ref. [16] although here we reiterate some relevant details for clarity of the present work.

## 2. Density matrix model

In our model, three consecutive periods of the QCL are considered. First, basis eigenstates are determined using a tight-binding Hamiltonian, in which each period of the QCL potential profile is “padded” within thick barriers such that the electrons are confined within a single period.

An extended Hamiltonian matrix is then generated to describe the interactions between each pair of states. The diagonal terms contain the state energies calculated using the tight-binding Hamiltonian, and the inter-period terms contain the Rabi oscillation strengths calculated as  $\hbar\Omega_{ij} \approx \langle i | H_{\text{ext}} - H_{\text{TB}} | j \rangle$  [17] where  $i, j$  are state indices and the terms  $H_{\text{ext}}$  and  $H_{\text{TB}}$  refer to the Hamiltonians (potentials) of the extended structure and of the “tight-binding” sections, respectively. Interaction with the light field present in the cavity is included in the Hamiltonian with off-diagonal intra-period terms given by [16]:

$$H_{i,j} = z_{i,j} A_0 e^{i\omega_0 t}, \quad (2)$$

where  $\omega_0$  is the frequency of the optical cavity field,  $t$  is time,  $z_{i,j}$  is the dipole matrix element for the transition, and  $A_0$  is the intensity of the cavity optical field.

Having specified the Hamiltonian matrix, the Liouville equation is then solved, as described in Ref. [16] to find the density matrix,  $\rho$ , which contains population and coherence information for three periods of the QCL structure. Inter-period coherences are calculated for all pairs of states, and this allows structures with many subbands to be modeled conveniently. Since it is not known in advance which states interact strongly with the optical field, each density matrix element is

assumed to have three harmonic terms such that

$$\rho_{i,j} = \rho_{i,j}^+ \exp(i\omega_0 t) + \rho_{i,j}^{\text{DC}} + \rho_{i,j}^- \exp(-i\omega_0 t). \quad (3)$$

A relaxation matrix is included in the Liouville equation, which describes the damping of the system. This contains both intra- and inter- subband lifetimes with scattering rate contributions from alloy disorder, acoustic phonons, longitudinal optical (LO) phonons and ionized impurities. Interface roughness scattering is also included with an r.m.s. roughness height  $\Delta=2.5 \text{ \AA}$  and correlation length  $\Lambda=100 \text{ \AA}$ , similar to that estimated elsewhere [18].

The current density is extracted from the solved density matrix as  $j = \text{Tr}(\rho J)/2$ , with the current matrix derived from the average drift velocity as

$$J = e \frac{i}{\hbar} [H, z], \quad (4)$$

where  $H$  is the Hamiltonian matrix,  $z$  is a matrix containing dipole transition elements, and  $e$  is the electron charge. Gain is extracted from  $J$  by calculating the complex permittivity as described in Ref. [16].

For each value of applied bias (field) a fully self-consistent simulation is performed and the light field strength ( $A_0$ ) iterated until gain is clamped to a defined loss. Variation of the cavity loss (and therefore the clamped optical field strength) affects current via the off-diagonal intra-period Hamiltonian terms in Eq. (2) which also affect the time-dependent coherences in Eq. (3). The intra-cavity optical power is calculated as

$$P = \frac{cnwh\epsilon_0}{2} |A_0|^2, \quad (5)$$

where  $\epsilon_0$ ,  $n$ ,  $w$ , and  $h$  are the vacuum permittivity, refractive index, width, and thickness of the active region respectively.

### 3. Free-running QCL characteristics

A BTC QCL emitting at 2.6 THz was driven using a dc current source. The device used here has the same active region design and semi-insulating surface plasmon waveguide as the structure described in Ref. [15], although was processed from a different wafer and with ridge dimensions  $2.4 \text{ mm} \times 150 \text{ \mu m} \times 11 \text{ \mu m}$ . The device was cooled using a continuous-flow helium cryostat and maintained at a constant heat-sink temperature of 35 K. Radiation from the laser was collimated using an off-axis paraboloidal (OAP) reflector and modulated at a frequency of 210 Hz using a mechanical chopper. The free-running relationship between THz power and bias voltage ( $P-V$ ) was measured by focusing the THz beam into a helium-cooled Ge:Ga photoconductive detector using a second OAP and recording the time-averaged signal via a lock-in amplifier synchronized to the modulation frequency. A THz photoacoustic power meter was used to calibrate measured values. The free-running current-voltage ( $I-V$ ) characteristics were recorded simultaneously.

Good agreement was achieved between the experimental  $P-I-V$  characteristics and our DM simulation by including a free-running loss of  $L_{\text{FR}} = 16.1 \text{ cm}^{-1}$ , an Ohmic contact resistance of  $1.57 \text{ \Omega}$  and photodetector collection efficiency of 48 %, as shown in Fig. 1 and included in Dataset 1 [19]. These simulations were carried out with a lattice temperature of 50 K to account for self-heating of the device. Although the carrier transport and light interaction characteristics of the DM model are shown to have good agreement with experimental data, some discrepancy with experiment is inevitable. Particularly important to this work is that current-driven QCLs will cease lasing when a negative differential resistance (NDR) region is reached. This is a known phenomenon caused by unstable oscillations between bias points that deliver the same drive current, and the resulting  $I-V$  curve appears to have a high gradient over this bias range.

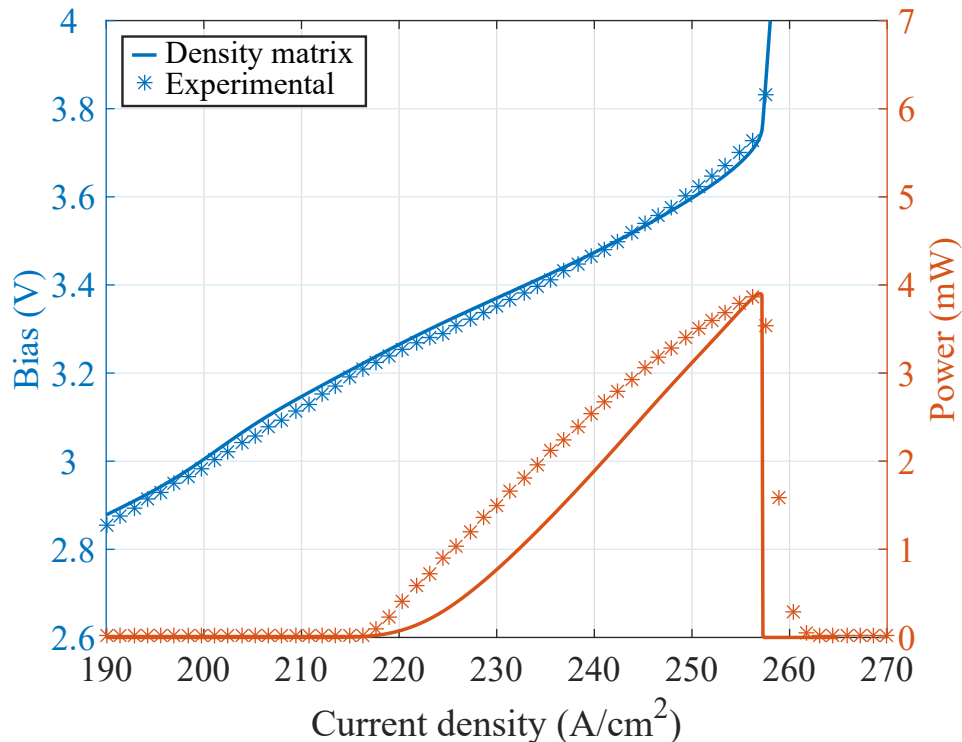


Figure 1. Comparison of calculated and experimental  $P$ - $I$  and  $V$ - $I$  curves for a heat sink temperature of 35 K. A contact resistance of  $1.57 \Omega$  is applied to the density matrix  $I$ - $V$  data simulated for a lattice temperature of 50 K.

To account for this in the model (in which the structure is biased with an applied field) the output power is set to zero, and current is asserted to increase a negligible amount (fitted with experiment), in NDR regions. Other experimental effects include contact resistance, contact voltage drops, parasitic currents and device heating. Therefore it can be necessary to link the current–light response calculated by the DM model with the measured  $I$ - $V$  curve. Current/loss dependencies of this “hybrid” approach are discussed further in Section 5.

#### 4. Self-mixing interferometry

An experimental LFI system was configured by reflecting the collimated THz beam back along the same optical path into the QCL cavity using a planar mirror, forming a nominal external cavity length of 40 cm. The resulting interference between the intra-cavity and reflected THz fields causes a small change in the emission frequency of the QCL such that the field is continuous across the facet-external cavity boundary. The feedback also gives rise to changes in the photon and electron density within the laser cavity, and this was observed as a perturbation to the terminal voltage  $V_{SM}$ , which was monitored via a lock-in amplifier synchronized to the chopper modulation frequency. In order to recover the maximum magnitude of voltage perturbation for each operating current, the phase of the reflected field was adjusted by varying the path length of the external cavity within one interference fringe.

We simulated the change in the internal cavity field due to optical feedback by introducing an equivalent change in cavity loss ( $\Delta L$ ) into our self-consistent model. This allowed for direct

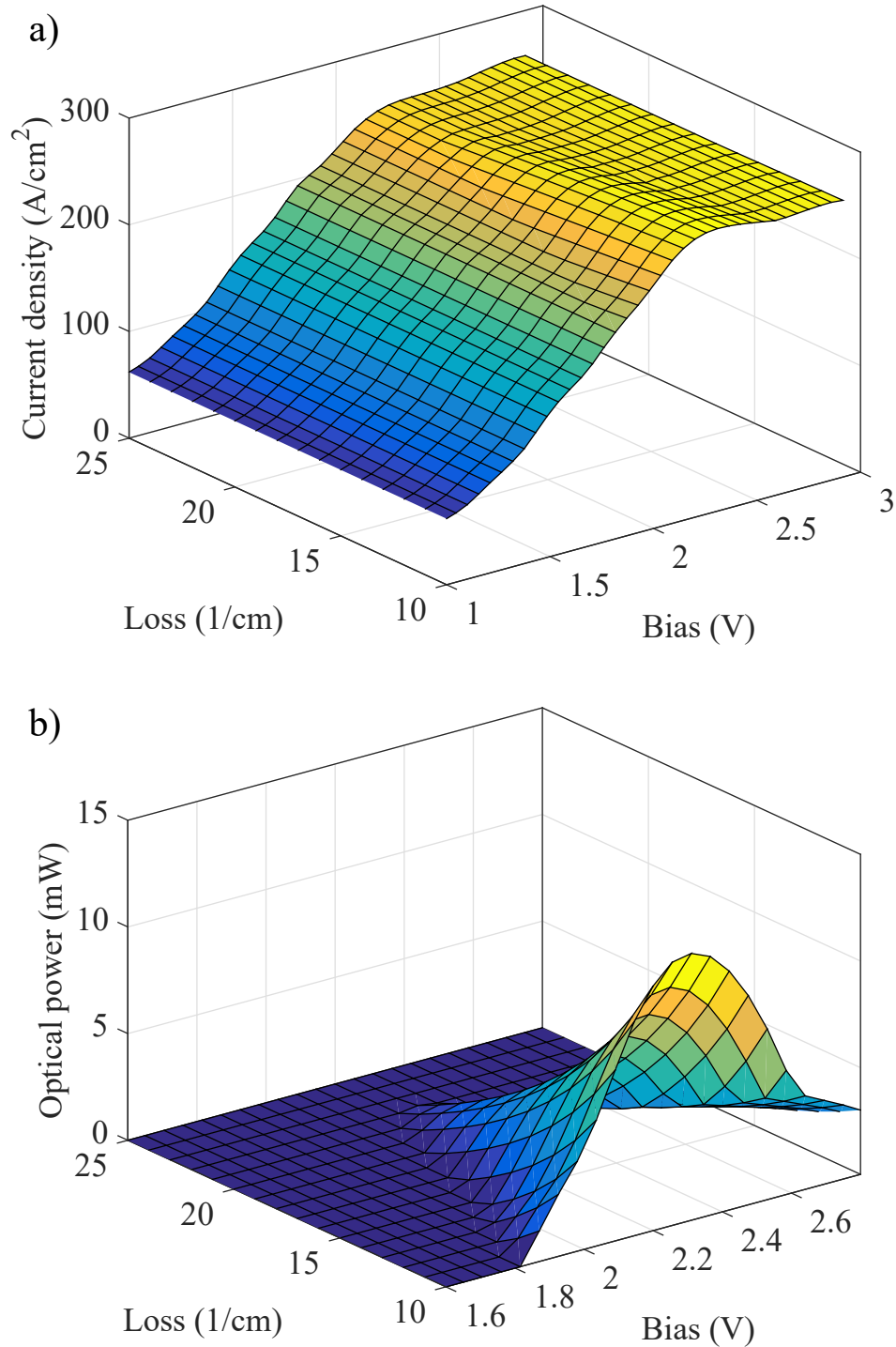


Figure 2. (a) Calculated current density and (b) optical power for QCL under lasing operation for a lattice temperature of 50 K. Changing cavity loss changes the threshold gain and lasing power which varies the photon driven current.

insight into the effects of the feedback level on the electron transport in the device and the resulting variations in the laser voltage and current. Experimentally, the QCL was driven at a fixed current and the terminal voltage was measured. However, in our electron transport model the applied field and cavity loss are inputs to the model, while current is a calculated output. To account for this an inverse interpolation of the bias–loss–current–density characteristic was performed to determine the equivalent field applied across the device for each current and cavity loss value. For example, if the QCL is lasing and cavity loss is decreased, then the optical field will increase to balance gain and loss. This increases stimulated emission current; however since the total current is fixed, the active region bias simultaneously decreases to compensate with decreased injection alignment. To obtain the computed data necessary for interpolation inversion, optical output power and current density were calculated between fields of 0–2.5 kV/cm and cavity losses of 10–25 cm<sup>-1</sup> (i.e. a range around the free-running loss determined in Section 3) and the results are plotted in Fig. 2. The self-mixing signal,  $V_{SM}$ , can then be obtained from interpolation of these data, at each current, as:

$$V_{SM}(I) = |V(I, L_{FR}) - V(I, L_{FR} + \Delta L)|, \quad (6)$$

where  $L_{FR}$  and  $\Delta L$  are the free-running loss and change in loss due to SM respectively. The appropriate value of  $\Delta L$  is dependent on the experimental setup and is affected by many factors such as the reinjection coupling efficiency, changing emission frequency, mode formation, and dynamic effects. Direct calculation of  $\Delta L$  is beyond the scope of the present work, where the origin of terminal voltage is of interest. The value of  $\Delta L$  is therefore chosen by fitting the magnitude of  $V_{SM}$  with experimental observations.

## 5. Results

Figure 3 shows experimental and theoretical  $V_{SM}(I)$  characteristics of the SM response. A fitted value of  $\Delta L = -1.4 \text{ cm}^{-1}$  is shown to provide excellent agreement for the signal amplitude over a large range of operating currents. Nevertheless, we note that  $\Delta L = -0.3 \text{ cm}^{-1}$  corresponds to a power modulation of approximately 5 %, which is consistent with that observed experimentally [13]. In both the simulated and experimental data, a strong enhancement of the SM signal occurs near where the QCL turns off due to the onset of the NDR region at  $I \approx 257 \text{ A/cm}^2$ .

We propose that the large  $V_{SM}$  signal observed here is due to the large QCL field perturbation required to achieve a subband alignment such that the total of the scattering/tunneling current and stimulated emission current remains equal to the drive current. It is noted that the theoretical model matches the experimental curve accurately up to the peak experimental value of  $V_{SM}=0.16 \text{ V}$ , which occurs around the switch-off current density ( $I \approx 257 \text{ A/cm}^2$ ). The theoretical model breaks down in the NDR region, with the theoretical value continuing to rise, and peaking at  $V_{SM} \approx 0.64 \text{ V}$ , whereas the experimental value decreases. This is attributed to the QCL becoming unstable experimentally in the NDR region. The smaller signal measured experimentally for larger currents ( $I > 257 \text{ A/cm}^2$ ) is likely due to the QCL operating intermittently.

With the mechanism of the relationship between  $V_{SM}$  and differential resistance established, it is appropriate to consider a simplified approach to its calculation. The rate of change of current with respect to loss predicted by the DM model was found to vary slightly over the ranges of bias and loss investigated. Instead, a typical value of  $dI/dL = 1.5 \times 10^{-4} \text{ kA/cm}$  can be used in conjunction with the experimental  $I$ – $V$  curve to calculate  $V_{SM}$  as

$$V_{SM}(I) = \left( \frac{dV_{FR}}{dI}(I) \cdot \frac{dI}{dL} \right) \Delta L, \quad (7)$$

where  $dV_{FR}/dI$  is the free-running differential resistance of the QCL. A comparison of this hybrid approach (for  $\Delta L = -0.5 \text{ cm}^{-1}$ ) with the experimental measurement is shown in Fig. 4.

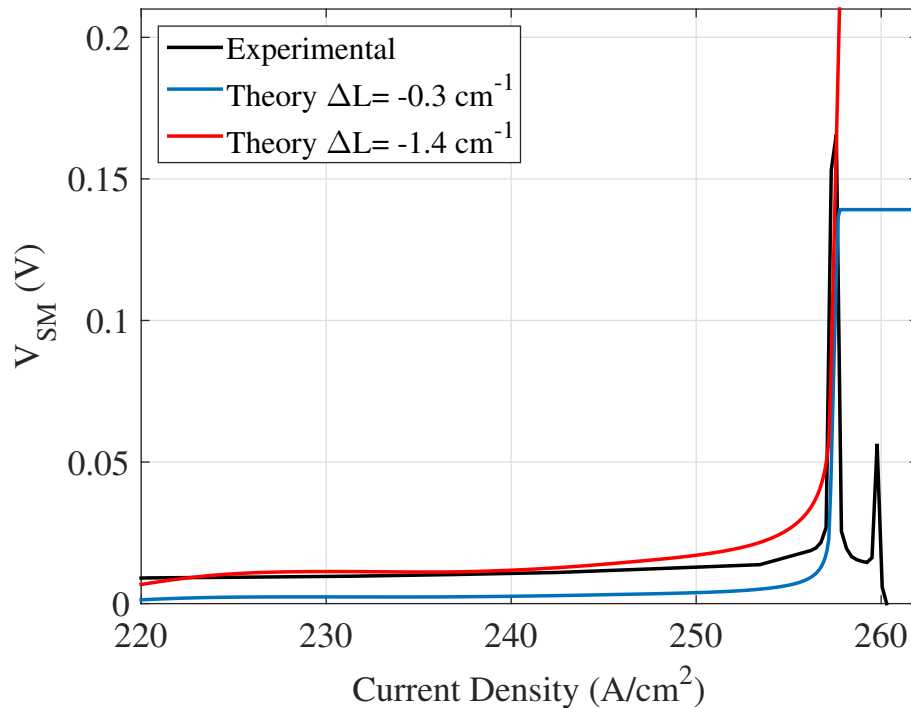


Figure 3. Comparison of peak SM terminal voltage signal calculated with an inverse interpolation of the density matrix model output, and experimental SM measurement.

This hybrid approach requires a lower loss value (compared to the previous purely-theoretical approach) in order to achieve the same signal amplitude due to the effect of contact resistance. In the purely theoretical model, the contact resistance shifts the voltage to greater values. However this has no effect on the self-mixing signal since drive current is fixed, and the voltage change due to contact resistance is therefore constant. However, in Eq. (7) the differential resistance term contains this voltage shifting effect, and therefore predicts a larger self-mixing signal.

The value of  $dI/dL$  will vary between different QCL devices depending mainly on the dipole matrix element of the upper-to-lower lasing level transition, doping density, and waveguide losses. This work suggests that QCLs that typically exhibit strong NDR regions, such as resonant LO phonon depopulated active regions may also exhibit sharp  $V_{SM}$  features such as that observed in this work. For swept-frequency SM approaches [20] in which the QCL drive current is swept, the signal could in principle be improved over a wide range of biases by optimizing the differential resistance through modification of the QCL design.

## 6. Conclusion

By applying a DM model of electron transport to a THz QCL device based on a bound-to-continuum structure, an explanation for the origin of terminal voltage variations due to optical feedback has been presented. Under feedback, the effective change in cavity loss results in a change in stimulated emission current. We propose that the bias voltage varies concurrently to maintain a constant drive current through the device under feedback. By combining experimental  $I$ - $V$  data of a QCL with DM output parameters excellent agreement is obtained for the magnitude and corresponding current density of the maximum self-mixing signal observed experimentally.

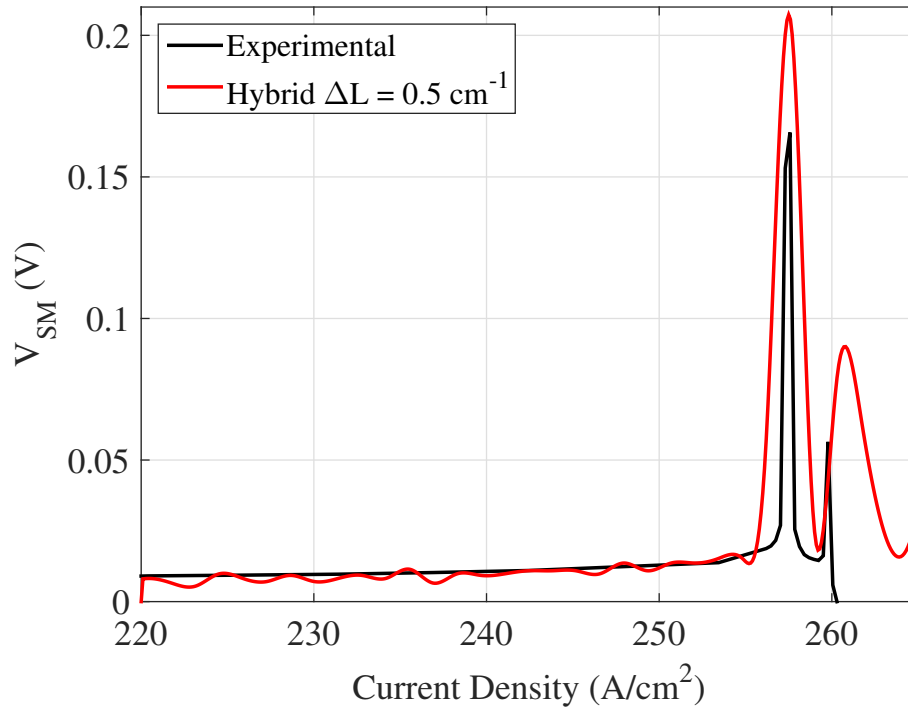


Figure 4. Comparison of experimental and “hybrid”  $V_{SM}$  results with a constant current–loss response of  $dI/dL = 1.5 \times 10^{-4}$  kA/cm.

This model could be used to design and evaluate QCLs tailored to provide enhanced feedback effects at desired wavelengths.

### Acknowledgements

This work was supported by Engineering and Physical Sciences Research Council (EPSRC) Grant COTS (EP/J017671/1); the Royal Society (UF130493) and the Royal Society Wolfson Research Merit Award scheme (A.G.D., E.H.L.)(UF130493); European Cooperation in Science and Technology (COST) (BM1205 and MP1204); and the Australian Research Council (DP160103910). A.G. acknowledges support from an EPSRC DTG award. P.D. acknowledges support from the EPSRC Fellowship scheme (EP/J002356/1). Y.L.L. acknowledges support under the Queensland Government’s Advance Queensland programme. Data associated with this paper are openly available from the University of Leeds data repository: <http://doi.org/10.5518/77>.